Article

Resonant Power Supply for Plasma Cleaning Based on Fuzzy Logic Power Tracking

Xiaowei Cai [1,*], Zhihe Fu [1], Huangsheng Xie [1], Jiaxiang Xue [2], Duhan Ding [2], Ning Ou [2] and Gang Zhou [3]

1 School of Physics and Mechanical and Electrical Engineering, Longyan University, Longyan 364012, China; fuzhihe@lyun.edu.cn (Z.F.); 81983005@lyun.edu.cn (H.X.)
2 School of Mechanical and Automotive Engineering, South China University of Technology, Guangzhou 510640, China; mejiaxue@scut.edu.cn (J.X.); daniel.din@foxmail.com (D.D.); 202120101055@mail.scut.edu.cn (N.O.)
3 Dongguan Large Electronics Co., Ltd., Dongguan 523070, China; zhougang@juda.cn
* Correspondence: 82013030@lyun.edu.cn; Tel.: +86-135-9962-3269

Abstract: The coaxial cylindrical reactor with a rotary nozzle is proposed to be used as the plasma torch of the plasma cleaning machine. The phase-shifted full bridge series resonance circuit is used as the power circuit topology. Because the voltage source load resonance circuit technology is mature, the cycle and difficulty of research and development on this basis are relatively small, and the corresponding control strategy and algorithm are relatively easy to achieve. At the same time, the voltage source circuit is smaller than the current source circuit, in line with the development trend of plasma cleaning equipment. In this paper, based on the phase shift full bridge series resonant circuit, the control strategy is compared and analyzed. Considering the response speed, control precision and efficiency, a PSPWM-PFM (Phase Shift Pulse Width Modulation- Pulse Frequency Modulation) hybrid modulation control strategy is proposed, which makes the system not only have a fast response speed but can also construct a soft switch and has a high efficiency. A maximum power tracking algorithm based on a fuzzy PFM was proposed to solve the problem that the plasma power supply deviated from the resonant frequency point easily due to environmental perturbation, and thus deviated from the maximum power point.

Keywords: plasma cleaning; fuzzy control; power tracking; resonant switching power supply; pulse frequency modulation

1. Introduction

The traditional cleaning methods mainly include mechanical cleaning, chemical cleaning, and ultrasonic cleaning. Mechanical cleaning is used for power tools or related equipment to remove rust, paint, and oxides on the surface of the object. The advantages are a simple operation and low technical requirements but can easily damage the object, for a complex shaped product is helpless, and the process to produce noise pollution, is not conducive to the operator and the health of the residents in the surrounding plants. Chemical cleaning uses chemicals to react with dirt or residue on the surface of the object, so as to achieve the purpose of cleaning. Chemical cleaning efficiency is high, can calmly deal with the appearance of complex products, and there is no noise pollution, but the disadvantages are the consumption of a large number of chemical reagents, it is easy to cause environmental pollution, and also may cause damage to the product itself, for some difficult to use wet cleaning products are powerless. Ultrasonic cleaning is to soak the product in the liquid, and make the liquid produce high frequency oscillation, generate shock waves, and remove the dirt on the surface of the object. This method has high pollution removal efficiency, but the disadvantage is that it also needs dry treatment, and the cleaning time should not be too long, otherwise it is easy to damage the cleaned object [1].

With the rapid development of industrial products, the continuous improvement of product quality, environmental protection awareness, and green energy saving awareness continues to be popular, and plasma cleaning will be widely used in the manufacturing industry. Plasma can be obtained by arc discharge, glow discharge, flame, laser or shock wave, etc., while the plasma used for cleaning belongs to low temperature plasma and is usually obtained by high-frequency and high-voltage breakdown gas. Depending on the cleaning object, different kinds of gas can be used, or the process can be completed in a vacuum environment. Although plasma cleaning has many of the advantages mentioned above, the current plasma power supply on the market has poor adaptability to generator load and cannot drive a variety of loads. There is a large loss of power from the supply system, a low power factor, the control ability of the plasma current variation is poor, and the system dynamic response is poor. Furthermore, the plasma power supply for an analog chip control power supply, single function, cannot meet the requirements of the application market control. Therefore, the power supply for plasma cleaning and its control strategy are studied in this paper [2–4].

2. Plasma Cleaning Power Supply Design

The nozzle of the plasma cleaning machine produces plasma by the electrical break-down of gas. For the plasma resonant power supply, the plasma torch is equivalent to a large capacitive load. If the pre-stage power supply is not properly compensated, the power factor will be too low affecting the efficiency, and the quality factor of the system will not be well controlled, while a small quality factor will cause a poor selectivity of the output power in frequency modulation [5].

Compensation for the capacitive load can be achieved by adding inductance to the primary side to form series resonance. In the case of a non-uniform electric field, the breakdown of 1 mm of compressed air needed for the breakdown voltage of about 3 kV, causes a lot of leakage inductance in the transformer. Now that the leakage inductance of the transformer is inevitable, simply using the series resonance with the load capacitance, can play a role of power factor compensation, and have a good quality factor. At the same time, it also avoids the volume increase caused by additional inductance.

The full-bridge inverter circuit is generally used to form high frequency and high voltage with a positive and negative polarity on the plasma torch. Although the traditional non-phase shifting control is simple, it is not convenient to construct a soft switch, and the switching loss is large. By adopting a phase shift full bridge control mode, the soft switch can be easily constructed, and the efficiency can be improved. Therefore, the phase-shifting full bridge is adopted as the control mode of the main circuit in this system [6].

The system architecture of the resonant power supply for plasma cleaning is shown in Figure 1, which mainly includes four parts: the power module, the control module, the auxiliary power module, and the human–computer interaction module.

The power module includes the front rectifier filter module, the phase shift full bridge circuit, and the high-frequency resonant transformer. The rectifier filter module is responsible for the power grid 220 V AC through the diode rectifier bridge and filter circuit to get smooth DC. The phase-shifting full-bridge circuit is responsible for inverting the DC obtained in the previous stage into a high-frequency AC square wave, acting on the high-frequency resonant transformer [7]. The high-frequency resonant transformer boosts the low-voltage AC square wave of the primary winding to the high-voltage AC square wave of more than 3000 volts of the secondary winding, and acts on the load discharge gun head, so that the gas of the gun head is continuously decomposed and generates plasma, which acts on the cleaning object.

The control module consists of signal detection and the conditioning circuit, the main control STM32 chip, and the phase shift full bridge driver circuit. The signal detection circuit is responsible for obtaining circuit voltage, current, and temperature information, and these analog signals through the conditioning circuit modulation output to the master chip. The master chip converts these analog signals into digital signals in the program

and calculates them to obtain the working condition of the plasma cleaning power supply system and controls the corresponding driving circuit accordingly to ensure the safe and stable work of the system.
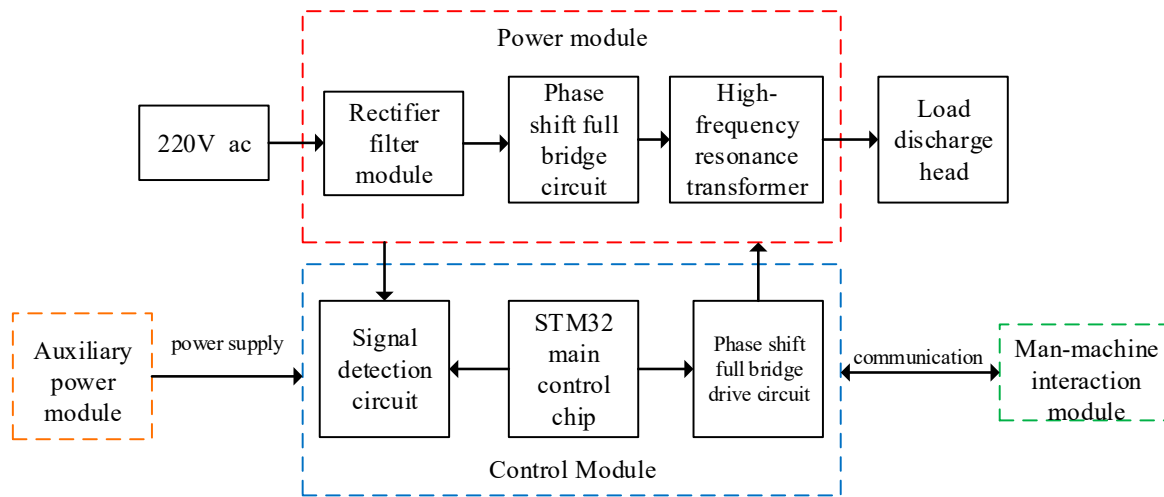
Figure 1. Structure of resonant power supply system for plasma cleaning.

The auxiliary power module is a multi-output quasi-resonant flyback circuit with UCC28610 as the control core, which supplies power to the circuits of different voltage levels such as the master chip, the signal conditioning circuit, and the drive circuit.

The human–computer interaction module is responsible for real-time communication with the main control chip to obtain the operation information of the plasma cleaning power supply system and display it through the control panel. Users can understand the real-time working conditions of the system through the panel and set the operation parameters through the operation control panel. The control panel will send these instructions to the main control chip, and then execute the corresponding control instructions.

This paper will analyze and design the resonant power supply system for plasma cleaning according to the system architecture mentioned above, and its main indicators are shown in Table 1.

Table 1. Performance index of resonant power supply system for plasma cleaning.

Performance Indicators	Performance Parameters	Parameters Unit
Input voltage range	198~242	V
Input current range	2.8~5	A
Input voltage frequency	50/60	Hz
Output voltage range	−3.2~3.2	kV
Output power	500~1000	W
Work efficiency	≥90	%

Figure 2 is the cross section of the resonant power supply plasma torch for plasma cleaning. By applying positive and negative pulses of high frequency and high voltage to the plasma torch, the working gas is continuously decomposed, and a filamentary plasma column is generated between the electrodes, which is blown away from the plasma torch under the action of gas pressure, thus generating plasma [8].

Plasma torch load is imposed by the working gas, nitrogen, argon, or compressed air. Nitrogen and argon gas on the material surface modification effect is better, but they are expensive, not suitable for mass production, and generally used in places that have requirements of specific requirements. Compressed air has a low cost and only needs a compressor to be achieved; therefore, it has been widely used in industry [9]. No matter what kind of gas is used, the gun head is equivalent to the capacitive load, so an equivalent

capacitance can be used to replace it in the circuit analysis, and the main circuit diagram of the system can be expressed, as shown in Figure 3. Wherein, L_{PLK} is the primary leakage inductance of the transformer, L_{SLK} is the secondary leakage inductance of the transformer, L_g is the inductance of plasma torch, R is the line resistance, and C_g is the equivalent capacitance of the nozzle air gap.
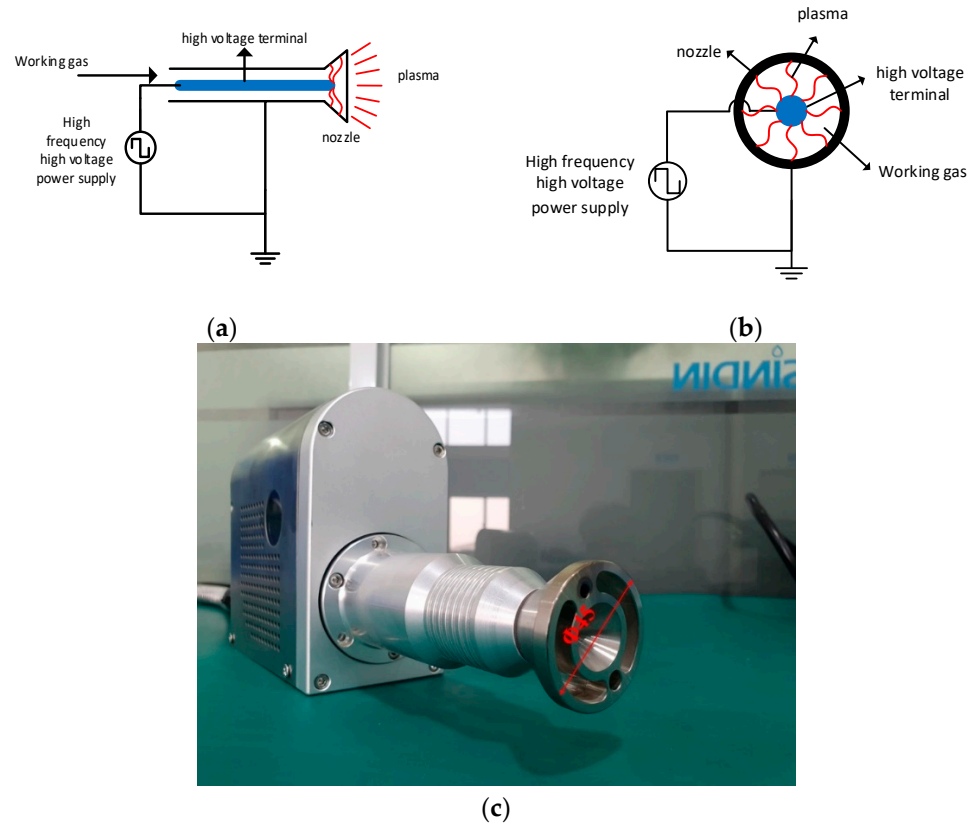

Figure 2. Cross section of plasma torch: (**a**) Lateral section; (**b**) Frontal section; (**c**) Real figure.
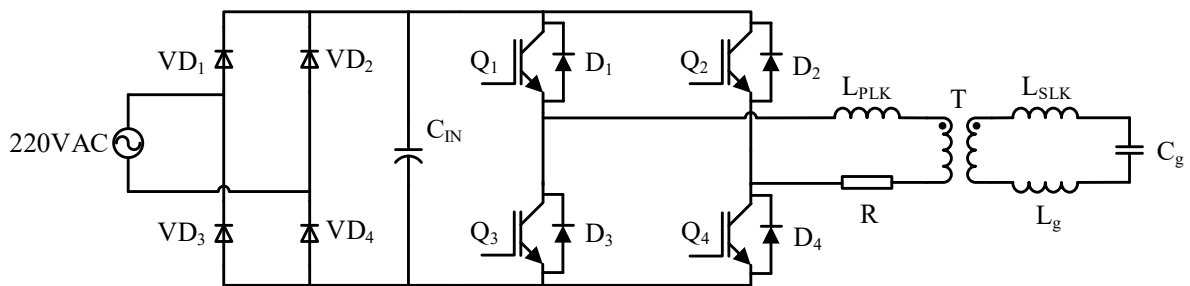

Figure 3. Main circuit diagram of resonant power supply for plasma cleaning.

The main control chip of the resonant power supply for plasma cleaning is STM32F103.

3. Resonant Power Supply Control Method for Plasma Cleaning

This section proposes a PSPWM-PFM hybrid modulation control mode, aiming to combine the characteristics of PSPWM and PFM control modes, so that the system can adjust the output power quickly and accurately, and ensure that the system has a wide enough power tuning range. It can also adjust the working frequency of the system to prevent the system from deviating from the resonant frequency point due to changes in the external environment such as air pressure, temperature, or load, and maintain a higher output efficiency.

Figure 4 shows the PSPWM-PFM mixed modulation closed-loop control diagram of the system. Firstly, the output voltage signal U and current signal I of the system are sampled. The voltage signal is obtained from the secondary winding of the power transformer and sampled by the secondary voltage detection circuit. The current signal is sampled by a secondary current detection circuit. After the signal is sampled and calculated by the master chip, the actual output power P of the system is obtained. The functions of over voltage protection (OVP), over current protection (OCP), and over power protection (OPP) are also set for the sampled and calculated signals. The actual output power P is compared with the user's set power PSET, and the power deviation E is obtained. After the PID modulation of bias E and mixed modulation of PSPWM-PFM, the driving signal with variable pulse width and period is obtained, and then the corresponding IGBT tube in the phase-shifting full-bridge circuit is driven to achieve the modulation of the output power [10,11].
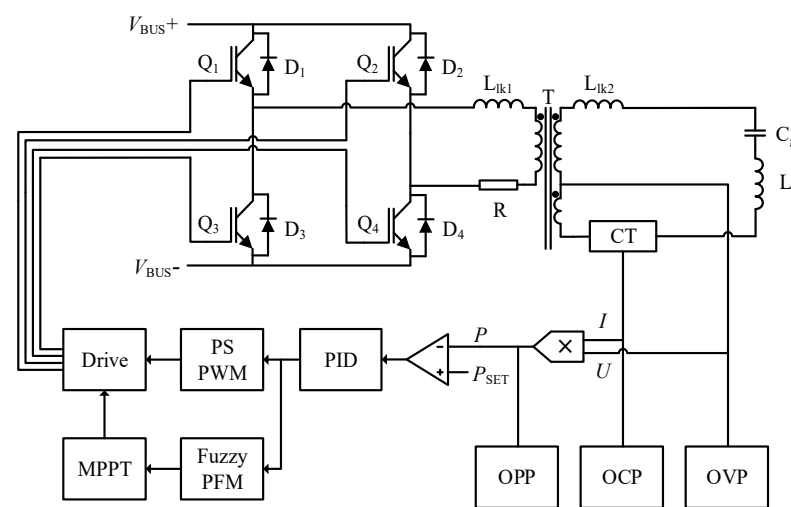
Figure 4. System mixed modulation closed-loop control diagram.

The program of the mixed modulation part of the main control chip is executed according to the flow chart shown in Figure 5. After the system is powered on, soft start is carried out first. After arcing successfully, the system allocates an initial duty cycle and frequency to the driver according to the set power. Then the operation according to the deviation between the actual power value and the set power value is selected. If the deviation is greater than 100 W, the system adopts PSPWM modulation. The adjustment time of the system is reduced by using the characteristics of PSPWM rapid power adjustment, so as to ensure that the system has a larger power adjustment range. If the deviation is less than or equal to 100 W, the system adopts fuzzy PFM modulation and carries out maximum power tracking to ensure that the system works at the maximum power point under the current duty cycle, namely the resonant frequency point, to ensure that the system has a high-power factor and work efficiency.

There are many ways to judge whether the system works near the resonant frequency point. One is to use the zero-crossing detection circuit to detect the zero-crossing of the secondary current of the transformer, and to ensure that the output current and voltage are in the same phase through the phase-locked loop, so as to ensure that the system works in the resonant state. However, for the plasma with a nonlinear working state, its load is always in a dynamic equilibrium state with large fluctuation, which is easy to cause the false zero-crossing detection and make the calculation result wrong [12].

Another simple and effective method is to continuously disturb the working frequency of the system, and record the corresponding working voltage and current, so as to find the working frequency corresponding to the maximum output power of the resonant power supply system for plasma cleaning. According to the simulation results, when the

system works near the resonant frequency, the active power output reaches the maximum value [13]. Its control flow chart is shown in Figure 6.
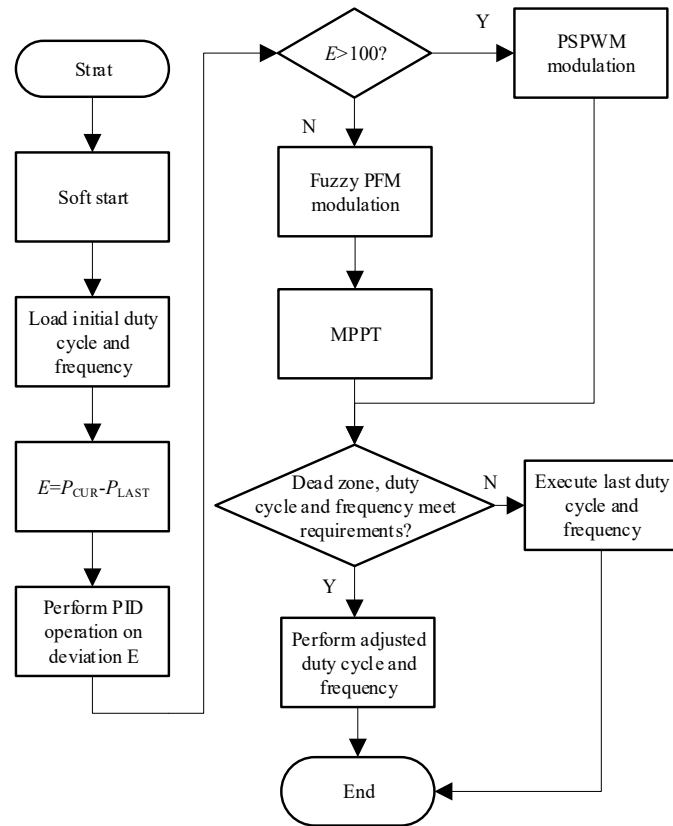

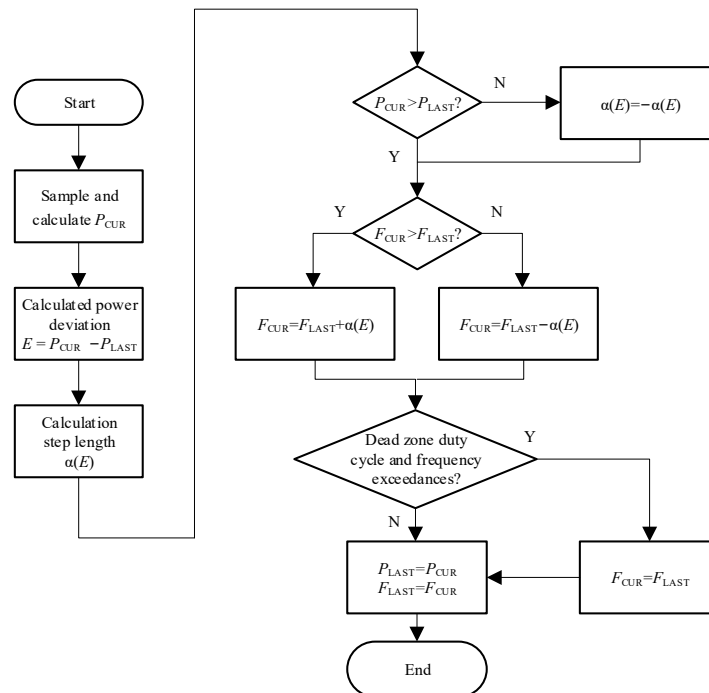**Figure 5.** Flow chart of PSPWM-PFM mixed modulation control program.

Figure 6. Flow chart of maximum power tracking program based on PFM.

The actual output power P_{CUR} is calculated according to the sampled output voltage and current, and the power change value E is obtained by comparing it with the power

at the last moment. Based on this, the disturbance step length α is calculated. Firstly, judge whether the current actual power P_{CUR} increases or decreases compared with the last power P_{LAST}. If it increases, the direction of disturbance is correct, and keep the direction of disturbance; otherwise, the disturbance will reverse. The increase or decrease of the frequency is determined according to the relationship between the current frequency F_{CUR} and the frequency F_{LAST} at the last time. Finally, judge whether the adjusted dead zone, duty cycle and frequency exceed the limit value. If not, the system will execute the adjusted frequency and update the power P_{LAST} and frequency F_{LAST} for the next calculation; otherwise, the frequency before the adjustment will be executed [14].

Although the PFM perturbation method has the advantages of being simple and efficient, it is difficult to achieve accurate and efficient power tracking for such a nonlinear time-varying system as a plasma discharge power supply. However, the fuzzy controller does not need an accurate mathematical model for the controlled object, so it is very suitable for this system. Therefore, the maximum power tracking algorithm based on fuzzy PFM is adopted in this paper to ensure that the system works near the resonant frequency point [15].

Figure 7 shows the working principle of the fuzzy controller. The system errors E and EC are obtained by the quantitative calculation of input and feedback, which are used as the input of the fuzzy controller. Control variables were fuzzified, fuzzy domains and corresponding membership functions were determined, and E and EC were obtained. Then, according to the pre-established fuzzy control rules, the decision is made, and the fuzzy output C is obtained. The fuzzy output C is de-fuzzified to obtain the actual control quantity C, which is sent to the control mechanism to complete the whole control process [16].
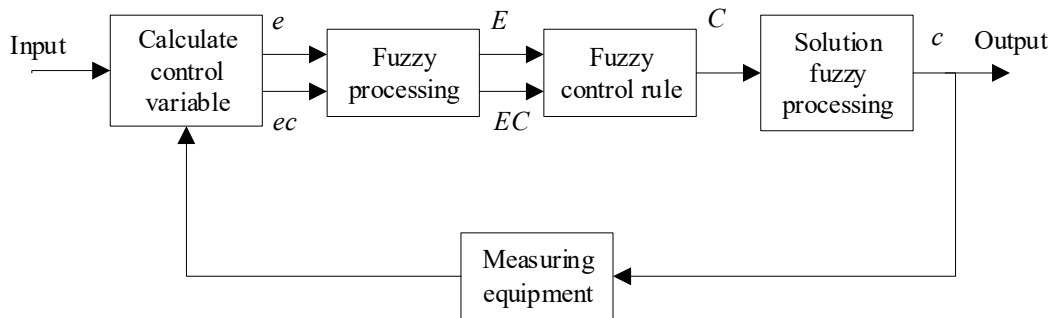

Figure 7. Fuzzy control principle.

The control variables of the algorithm are system output power and frequency, respectively. The input *e* and *ec* of the fuzzy controller are their corresponding changes, namely:

$$e = P(k) - P(k-1) \tag{1}$$

$$ec = F(k) - F(k-1) \tag{2}$$

The output parameter *c* is the disturbance amount to the driving signal frequency of the full-bridge switch tube, namely:

$$c = \Delta F_D \tag{3}$$

The fuzzy theory domain of input *e*, *ec*, and output *c* is set as $E = EC = C = [-1, -0.8, \ldots, 0.8, 1]$, with a total of 11 grades. The value of parameter variation and control quantity can be expressed by fuzzy subsets. The fuzzy subsets of power variable e and output control variable *c* are represented by seven fuzzy languages: "positive big (PB), positive median (PM), positive small (PS), zero (ZE), negative small (NS), negative medium (NM), and negative big (NB)". EC, the fuzzy subset of frequency variation, is expressed by six fuzzy languages: "PB, PM, PS, NS, NM, NB". The relationship between each input quantity and each fuzzy subset is represented by membership function. Membership curves of *E*, *EC*, and *C* are shown in Figure 8.
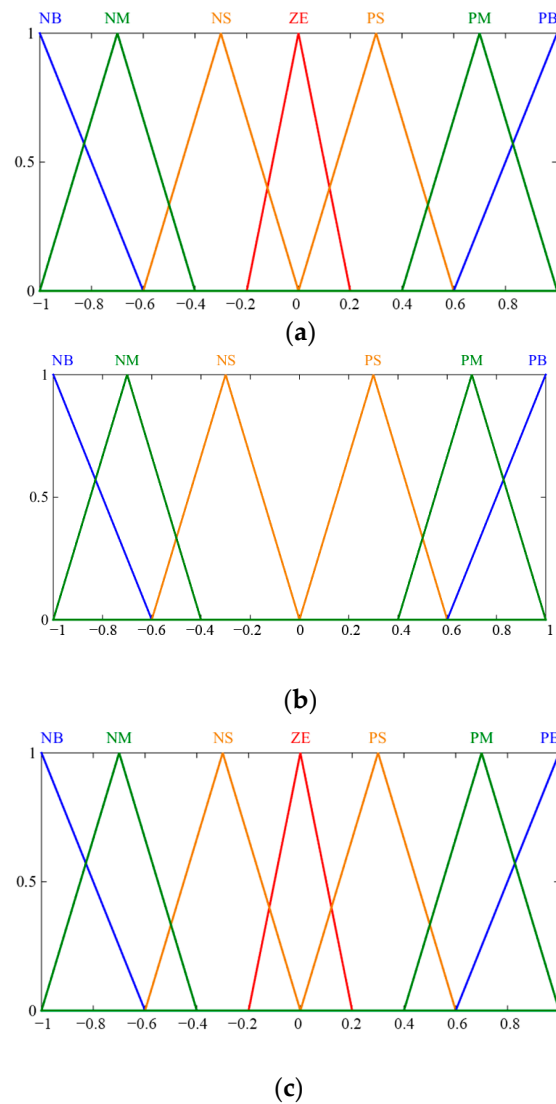
Figure 8. Membership degree curve: (**a**) Membership curve of *E*; (**b**) Membership curve of *EC*; (**c**) Membership curve of *C*.

After the fuzzy processing is completed, the corresponding fuzzy control rules can be formulated. They are formulated according to human experience. The design idea is: when the power change is positive, the disturbance direction is proved to be correct, and the direction of output control quantity and frequency change quantity should be consistent, otherwise, the reverse operation should be carried out. The control quantity is consistent with the power change quantity, that is, when the system is close to the maximum power point, the power change quantity is small, and the disturbance quantity should be kept small, otherwise the control quantity should be kept large. The fuzzy control rules are shown in Table 2 and Figure 9, and the corresponding 3D surface of the fuzzy control rules is shown in Figure 8 [17].

Table 2. Fuzzy control rules.

EC	E						
	NB	**NM**	**NS**	**ZE**	**PS**	**PM**	**PB**
NB	PB	PM	PS	ZE	NS	NM	NB
NM	PB	PM	PS	ZE	NS	NM	NB
NS	PB	PM	PS	ZE	NS	NM	NB
PS	NB	NM	NS	ZE	PS	PM	PB
PM	NB	NM	NS	ZE	PS	PM	PB
PB	NB	NM	NS	ZE	PS	PM	PB
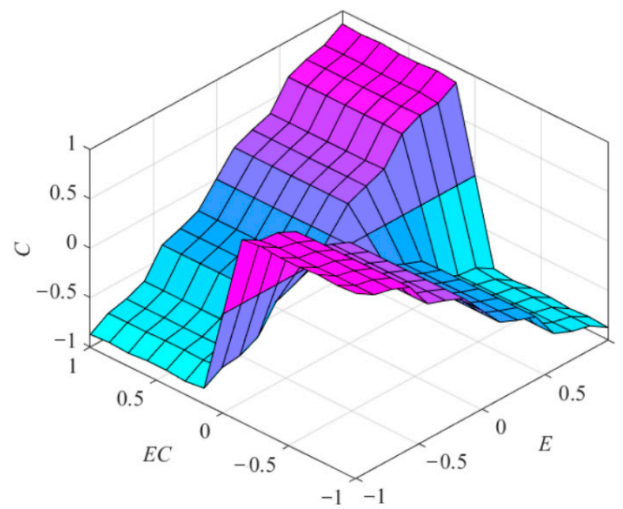
Figure 9. 3D output surface of fuzzy control rules.

After the above steps, the output quantity C needs to be de-fuzzified and converted into the actual control quantity, so as to realize the modulation of the driving frequency. In this paper, the gravity center method is adopted to solve the ambiguity, and its formula is:

$$c = \frac{\sum\limits_{i=1}^{n} \mu(U_i)U_i}{\sum\limits_{i=1}^{n} \mu(U_i)} \tag{4}$$

where, c is the output of the fuzzy controller, U_i is the center value of the output corresponding to the membership function interval, and $\mu(U_i)$ is the membership degree corresponding to U_i [18].

A model is built in Simulink to simulate the above hybrid modulation algorithm and the maximum power tracking algorithm based on fuzzy PFM, as shown in Figure 10. The upper part of the figure consists of the main circuit of the phase-shifted full bridge and its load. In order to simulate the mutation of the load caused by perturbation, capacitors C_1 and C_2 are connected in parallel or in series at the equivalent load. They are controlled by pulse signals G_1 and G_2 and switch transistors Q_5 and Q_6, respectively, so as to introduce perturbation at specific time points. The lower part is a hybrid modulation algorithm, including a frequency estimator, a PSPWM controller, a fuzzy PFM controller, and a drive signal generator.
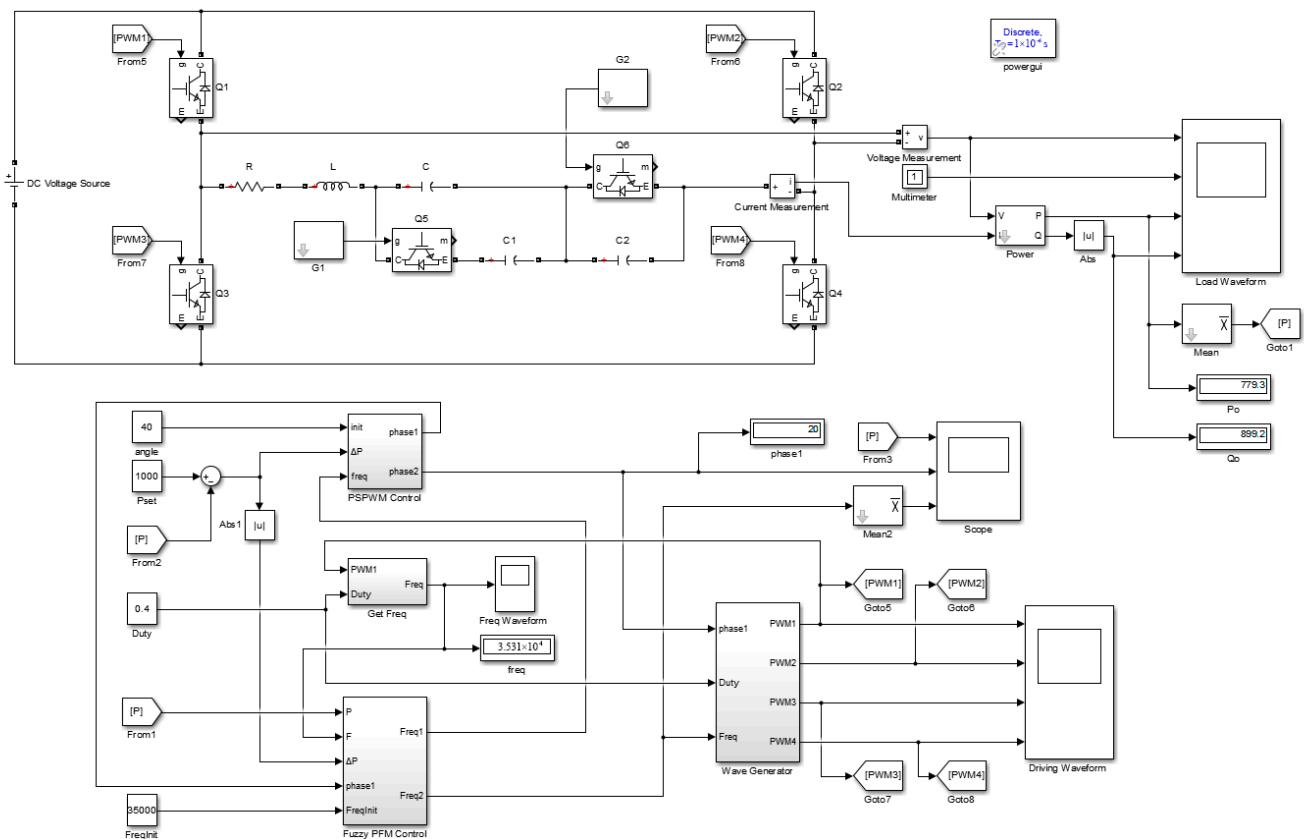
Figure 10. Simulation model of hybrid modulation algorithm.

Figure 11 shows the internal structure of a frequency estimator. This circuit is used to obtain the working frequency of PWM. Firstly, the single PWM (Pulse Width Modulation) waveform is integrated, and then the peak point is sampled by the delay circuit and comparison function. Finally, the working frequency of the corresponding time point is derived by the duty cycle.
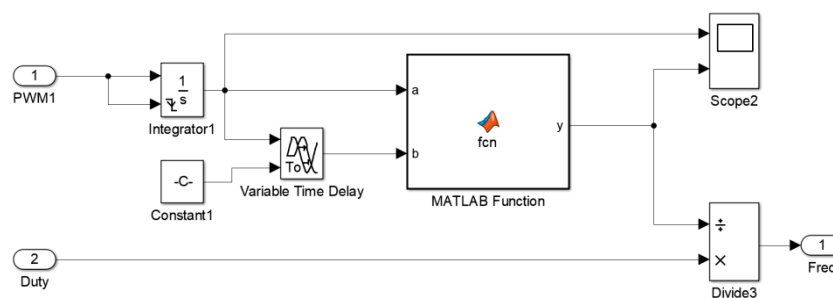

Figure 11. Internal structure of the frequency estimator.

Figure 12 shows the internal structure of a PSPWM controller. The module detects the frequency and power error of the system in real time. Once the power error is above 100 W, or the frequency deviates to the upper and lower limits during frequency modulation, namely 2.5 Hz and 6.5 kHz, the module starts to work and realizes power control by adjusting the phase shift angle [19].
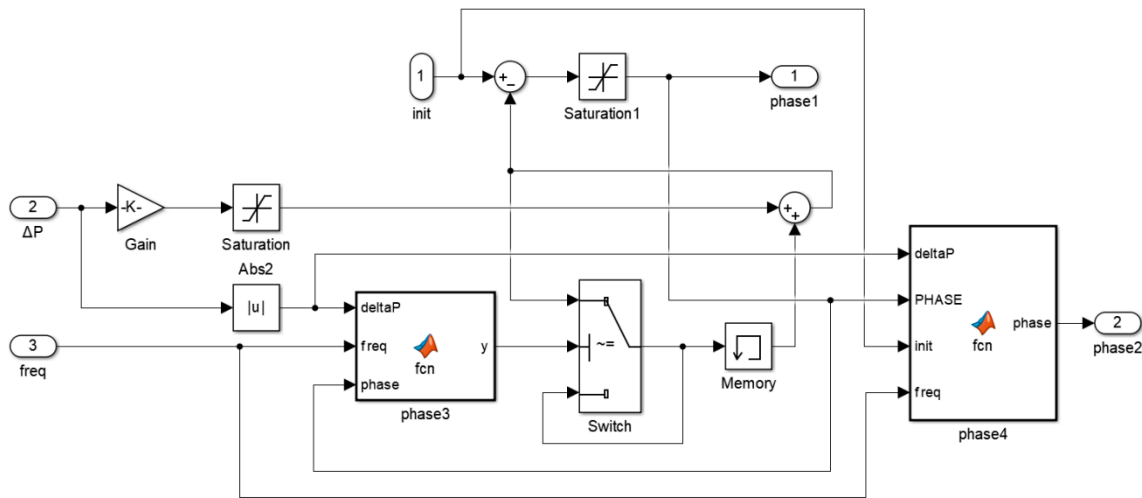
Figure 12. Internal structure of a PSPWM controller.

The internal structure of the fuzzy PFM controller is shown in Figure 13. Firstly, the power and frequency of the system are sampled and preprocessed, and the variation value is obtained and input into the fuzzy controller. The output value, as the variation of frequency, is added to the initial frequency and sent to the PFM modulator. When the power error is less than 100 W, or the phase shift angle deviates to $20°$ or $70°$, the module starts to work to realize the maximum power tracking under the current duty cycle of the system, prevents the system from deviating from the resonant frequency due to external perturbation, and ensures the working efficiency of the system.
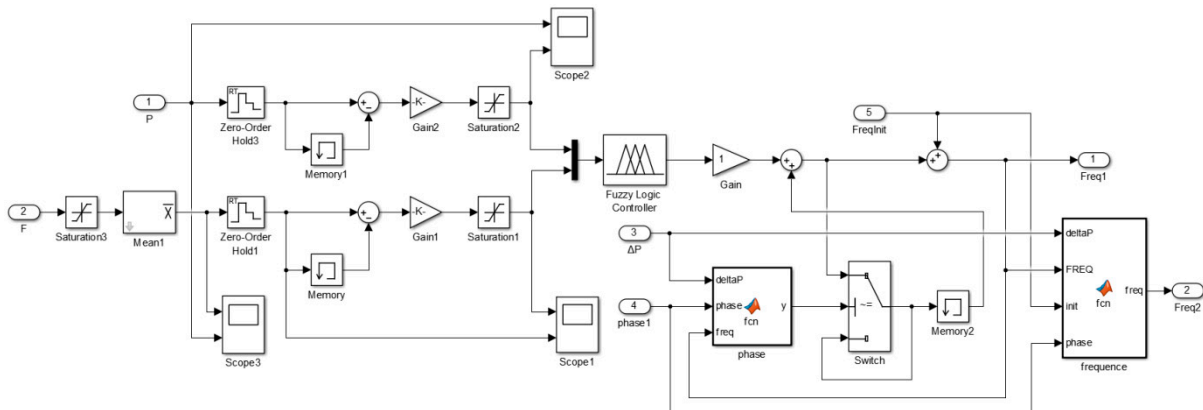

Figure 13. Internal structure of a fuzzy PFM controller.

Figure 14 shows the internal structure of the driver signal generator. The module uses an integrator and flip comparator to convert the adjustable digital input signal into an adjustable triangular wave signal, and then compares the triangular wave with the duty cycle signal to generate a pulse waveform with an adjustable frequency. A delay device is used to generate a four-channel PWM waveform with a phase shift angle, which is used to drive the full-bridge circuit [20].
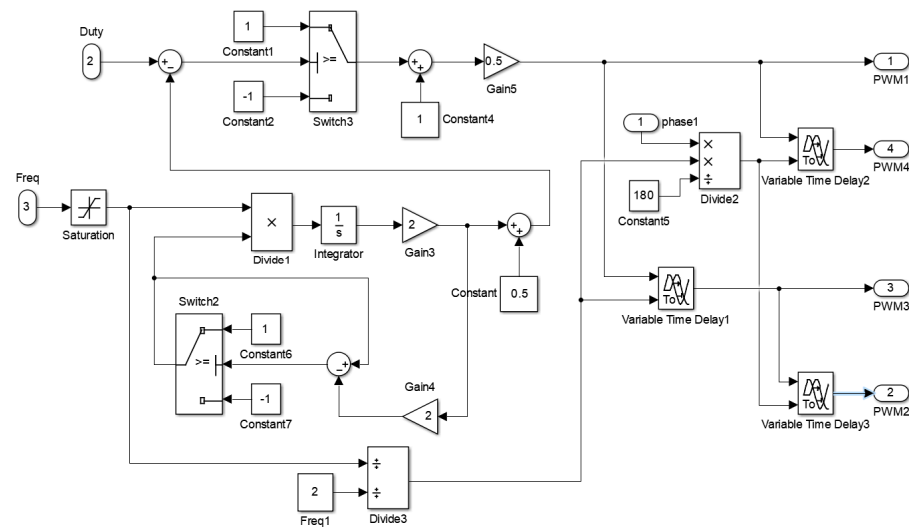
Figure 14. Internal structure of the driver wave generator.

Adjust the equivalent load of the system, set the resonance frequency of the system as 42.54 kHz, the initial operating frequency as 35 kHz, the initial phase shift angle as 45°, the duty cycle as 0.4, and the output power as 1000 W to simulate the system. Figure 15 shows the output power, phase shift angle, and operating frequency. As can be seen from the figure, after 0.05 s, the output power of the system is stable at about 1000 W, the phase shift angle is stable at 53°, and the working frequency is stable at about 40 kHz. It can be seen that the hybrid modulation algorithm has the advantages of a fast adjustment speed, a high-adjustment precision, and is operable.

Figure 15. Simulation waveform of hybrid modulation algorithm.
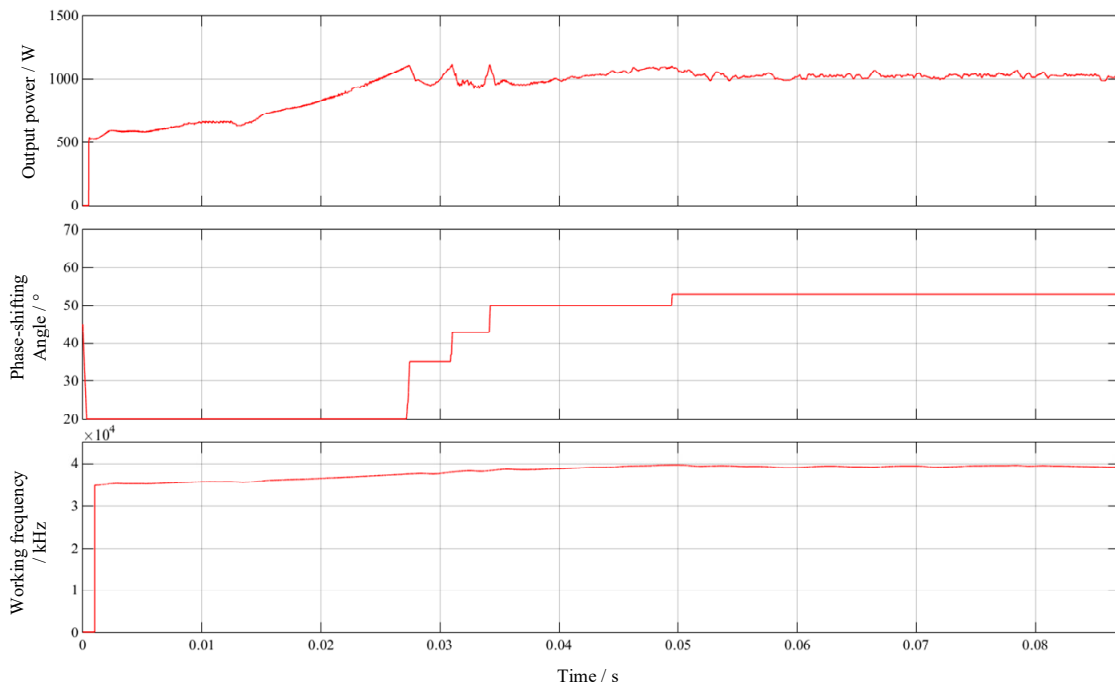
Set the initial operating frequency of the system as 40 kHz, the initial phase shift angle as 55°, the duty cycle as 0.4, and the target output power as 1000 W. At 0.05 s, the parallel capacitor C_1 perturbation is introduced, and its capacitance value is 25 nF, that is, the equivalent load capacitance of the system increases from 35 nF to 60 nF at 0.05 s, and

the anti-perturbation performance of the system is simulated. Figure 16 shows the output power, phase shift angle, and operating frequency.
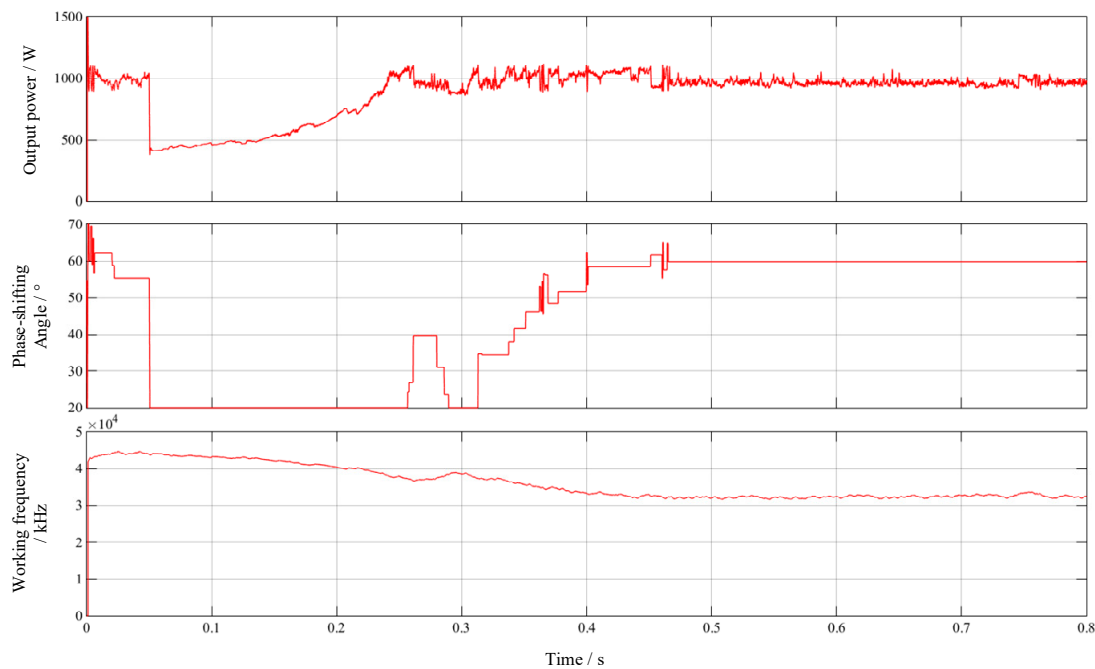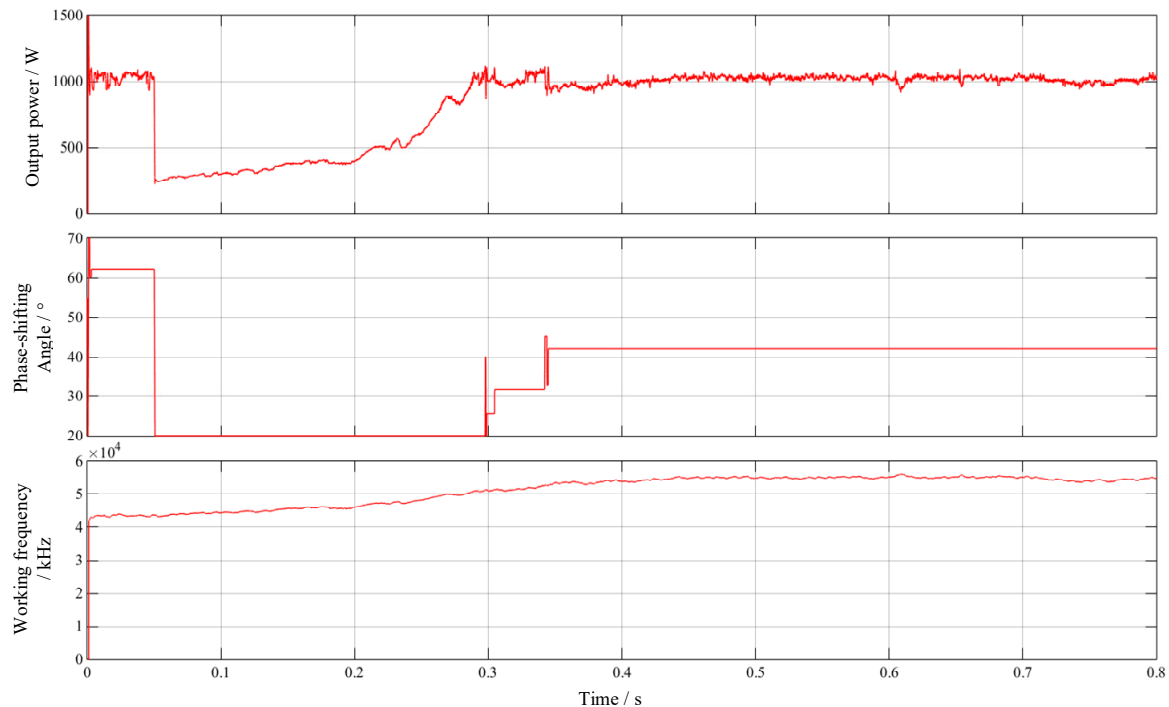

Figure 16. Anti-perturbation waveform of load capacitance surge.

As seen in Figure 16, at 0.05 s the load capacitance spurts resulting in the system and the resonance frequency of the power of the output power falling sharply. The error of the algorithm to detect the output power is very big and tries to improve the power output by rapidly reducing the phase-shifting angle. When the phase-shifting angle adjustment to the lower limit of 20° still cannot meet the needs of power set, the maximum power tracking algorithm based on fuzzy PFM starts to work. During the period of 0.05 s to 0.25 s, the operating frequency of the system decreases, and the resonant frequency point is constantly approached, so that the output power increases. During the period from 0.25 s to 0.46 s, the working frequency continues to decrease and approach the resonant frequency, so as to maintain the maximum efficiency of the plasma power supply, but the output power should be stable at 1000 W and cannot continue to rise. At this time, PSPWM takes effect, making the working frequency track the resonant frequency point while the output power remains stable. Finally, after 0.46 s, the output power, phase shift angle, and operating frequency of the system stabilize at about 1000 W, 60°, and 32 kHz, respectively.

Under the same conditions, the C_2 perturbation of the series capacitor is introduced at 0.05 s with a capacity of 46 nF, that is, the equivalent load capacitance of the system drops from 35 nF to 19.88 nF at 0.05 s. The anti-perturbation performance of the system is simulated, and the simulation results are shown in Figure 17.

As can be seen from Figure 17, at 0.05 s, the sudden change of load leads to a sharp decline in system output power, and the phase shift angle is rapidly adjusted to the lower limit of 20°, but the actual output power is still too small. The maximum power tracking algorithm based on fuzzy PFM takes effect at this time. From 0.05 s to 0.3 s, in this period of time the working frequency continues to rise close to the resonant frequency point, and the output power increases to about 1000 W. During the period from 0.3 s to 0.35 s, the working frequency continues to rise, but the output power should be stable at 1000 W. At this time, PSPWM takes effect and keeps the output power stable by increasing the phase shift angle to offset the influence of frequency increase on the output power. Finally, after 0.35 s, the output power, phase shift angle, and operating frequency of the system stabilize at about 1000 W, 42°, and 55 kHz, respectively.

To sum up, the PSPWM-PFM hybrid modulation algorithm has the characteristics of a fast response speed and a high adjustment accuracy, while the maximum power tracking algorithm based on fuzzy PFM enables the system to have the ability of self-correction when disturbed, so that the system keeps working near the resonant frequency point with high efficiency. Therefore, the application of this algorithm in the field of resonant power supply for plasma cleaning is feasible.

Figure 17. Anti-perturbation waveform when the load capacitance drops sharply.

4. Analysis of Test Results

Based on the hardware circuit design and control strategy analysis in the previous sections, the prototype is developed, and the corresponding experimental platform is built. The key circuit point waveform of the prototype was tested, and the power regulation experiment was conducted to verify the relationship between the output active power, phase shift angle, and working frequency. The performance of three different modulation methods were compared and tested to verify the advantages of the hybrid modulation algorithm in the comprehensive efficiency, and the cleaning effect of the plasma cleaning machine was tested. At the same time, the influence of various factors on the cleaning effect of plasma cleaner is verified.

Figure 18 shows the main circuit board of the resonant power supply system for plasma cleaning, which is designed according to the idea of modularization, including the rectifier filter circuit, the auxiliary power supply, the driving circuit, and the phase shift full bridge circuit of the front stage. The auxiliary power supply adopts a plug-in board mode, which makes full use of the longitudinal space and reduces the area of the prototype.

Figure 19 shows the experimental platform of the resonant power supply system for plasma cleaning. The experimental instruments mainly include an air compressor, a four-channel oscilloscope, a programmable AC power supply, a contact angle measuring instrument, a multimeter, an ultra-high voltage probe, a differential probe, and a current probe, etc. Using a rotating jet plasma head, the discharge situation of the plasma jet during operation is shown in Figure 20.

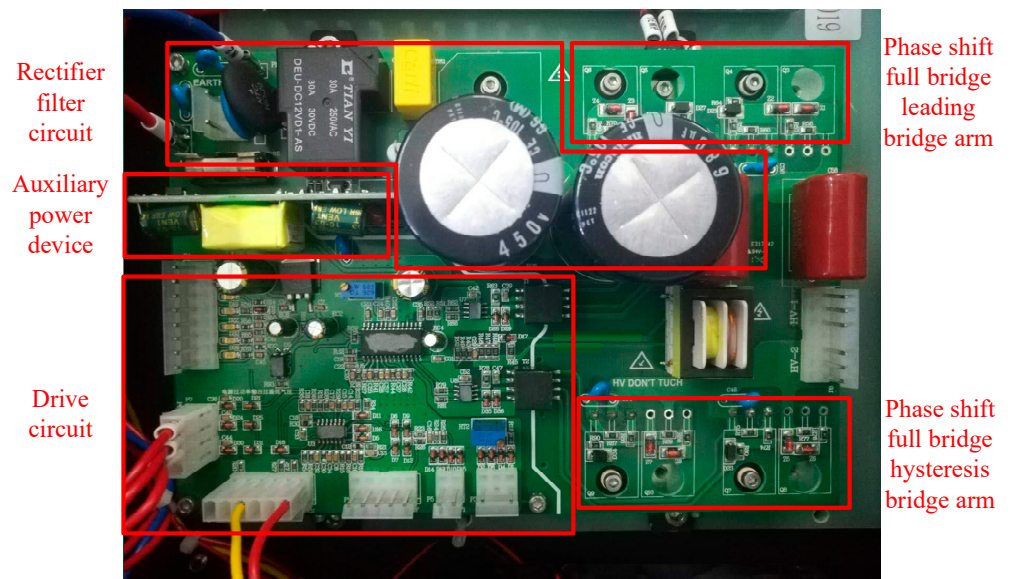**Figure 18.** Main circuit board of resonant power supply system for plasma cleaning.

Figure 19. Experimental platform of resonant power supply system for plasma cleaning.
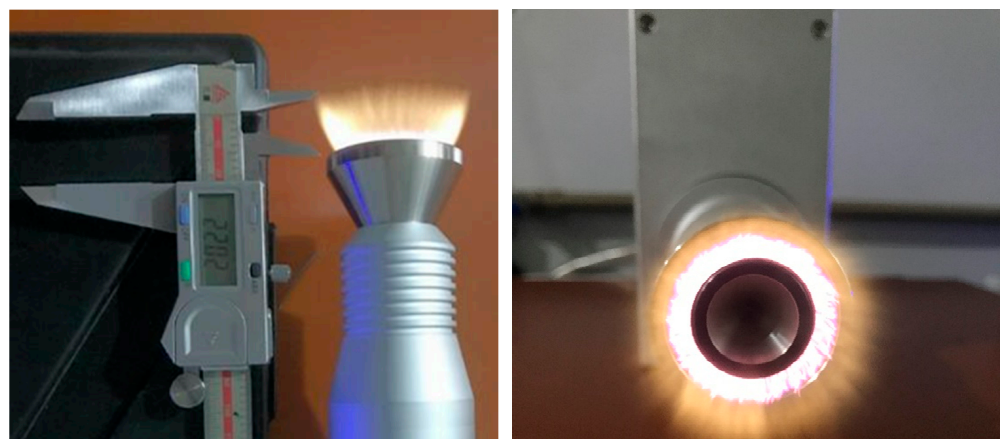

Figure 20. Discharge situation of plasma jet during operation.

In order to verify whether the theoretical analysis and simulation of the relationship between output active power, phase shift angle, and frequency are correct, the operating frequencies of the system are set to fixed values, respectively: 20 kHz, 25 kHz, 30 kHz, 35 kHz, 40 kHz, 45 kHz, and 50 kHz. Meanwhile, the phase shift angle from 10° to 130° every 10° was adjusted, and the output power of the plasma prototype when working at different frequencies and phase shift angles was recorded. The test results are shown in Table 3. For data lower than 500 W, due to an unstable plasma arc, the table does not record data exceeding 1000 W are not recorded in the table because overload protection is triggered.

Table 3. Power regulation test data table.

Phase-Shifting Angle (°)	Output Power (W)						
	20 kHz	25 kHz	30 kHz	35 kHz	40 kHz	45 kHz	50 kHz
10	958	-	964	922	861	798	723
20	950	990	952	919	851	781	718
30	937	979	931	900	823	756	707
40	918	958	895	882	814	740	696
50	886	935	871	860	796	720	678
60	877	893	853	840	775	700	660
70	837	869	830	825	755	673	627
80	820	850	810	790	725	640	605
90	785	810	773	770	678	605	565
100	720	755	705	740	636	560	530
110	653	690	640	625	605	510	490
120	578	625	560	580	545	-	-
130	500	545	490	540	-	-	-

The data in the table are sorted into curves as shown in Figure 21, and the following conclusions can be drawn from the analysis:

(1) At the same working frequency, the larger the phase shift angle of the system is, the lower the output power is; the smaller the phase shift angle of the system is, the higher the output power is.

(2) The four curves of 20 kHz, 25 kHz, 30 kHz, and 35 kHz are relatively dense, that is, the resonant frequency of the system jitter in the range of 20 kHz–35 kHz.

(3) At the same phase shift angle, the closer the operating frequency of the system is to the resonant frequency, the higher the output power of the system will be; otherwise, the lower the output power will be.

(4) Pure PFM regulation, that is, in the fixed phase shift angle frequency modulation mode, the power range is narrow, not more than 300 W, which is the shortcoming of pure PFM modulation mode; similarly, pure PWM adjustment, that is, in the fixed frequency adjustment phase shift angle, the power range can not fully meet the requirements.

(5) The curve is steeper when the phase shift angle is larger, and is slower when the phase shift angle is smaller. That is, the larger the phase shift angle is, the greater the influence of the phase shift angle on the output power is; otherwise, the smaller the influence is, which is consistent with the simulation results. Other factors contributing to this phenomenon are as follows: the smaller the phase shift angle is, the phase shift full bridge will gradually separate from the soft switch and become the hard switch, leading to the increase in switching loss of the power tube, thus offsetting part of the increased output power. Therefore, in order to maintain a high output efficiency, it is not advisable to adjust the phase shift angle too small in actual modulation.
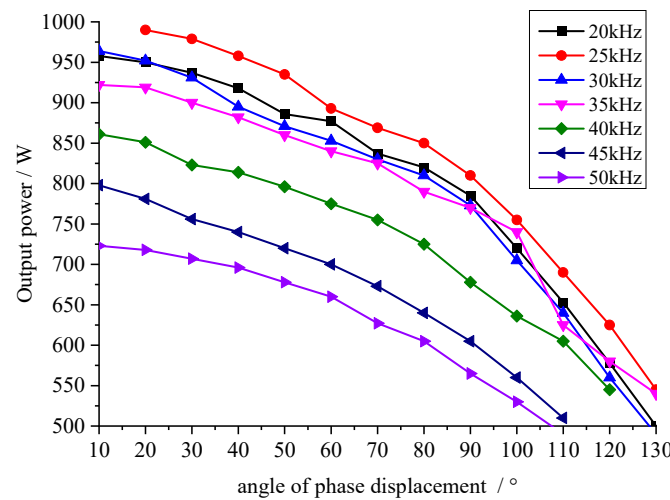
Figure 21. Diagram of the relationship between output power and phase shift angle.

In order to verify the PSPWM-PFM hybrid modulation algorithm, compared with the pure PWM modulation or PFM modulation, the comprehensive efficiency is higher, and the power matching accuracy is also higher. Test the resonant power supply system for plasma cleaning, respectively, input power and output power in PSPWM-PFM, PWM and PFM modulation modes, and record the relevant experimental data, as shown in Table 4.

Table 4. Algorithm performance test data table.

Setting Power (W)	PSPWM-PFM		PWM		PFM	
	Input Power (W)	Output Power (W)	Input Power (W)	Output Power (W)	Input Power (W)	Output Power (W)
500	573.5	476.6	-	-	681.4	579.9
550	600.5	498.2	-	-	686.2	583.3
600	653.8	547.3	744.6	588.8	662.3	569.1
650	713.1	613.3	805.6	663.9	669.8	572.0
700	758.2	663.4	834.8	696.6	674.1	587.8
750	803.2	706.8	875.2	746.6	698.3	615.2
800	828.6	736.6	888.8	781.6	766.1	671.9
850	865.1	792.4	964.2	823.3	774.4	705.5
900	905.8	829.7	1021.9	893.1	791.9	729.3
950	923.9	859.7	1073.52	954.9	828.3	769.5
1000	968.1	926.4	-	-	837.3	780.4

In Table 4, there are three groups of experimental data that are not recorded, namely: when the power is set to 500 W, the experimental data are difficult to record because the PWM algorithm fails to start the arc; when the power is set as 550 W, the experimental data cannot be recorded because of the unstable arc of the PWM algorithm; when the power is set to 1000 W, the experimental data will not be recorded because the PWM algorithm triggers over power protection.

Based on the input power and output power data recorded in Table 4, you can calculate the efficiency curves of the three modulation modes at each set power, as shown in Figure 22. As can be seen from the figure, the efficiency of the PWM modulation mode is the worst among the three, and the lowest efficiency is less than 80%, especially in low power and high-power operation. This is because the PWM cannot adjust the frequency and it is easy to deviate from the resonant frequency point of the system, so that the system has too much reactive power, resulting in a low efficiency. The PFM modulation mode and the hybrid modulation mode have their own advantages and disadvantages in each set power, but at low power operation the PFM modulation mode has better efficiency than

the hybrid modulation mode because of its frequency modulation characteristics. Among them, the PFM modulation efficiency is above 85%, and the mixed modulation efficiency is above 83%, which meet the requirements. Regardless of the modulation mode, the overall efficiency of the system tends to increase as the set power increases.
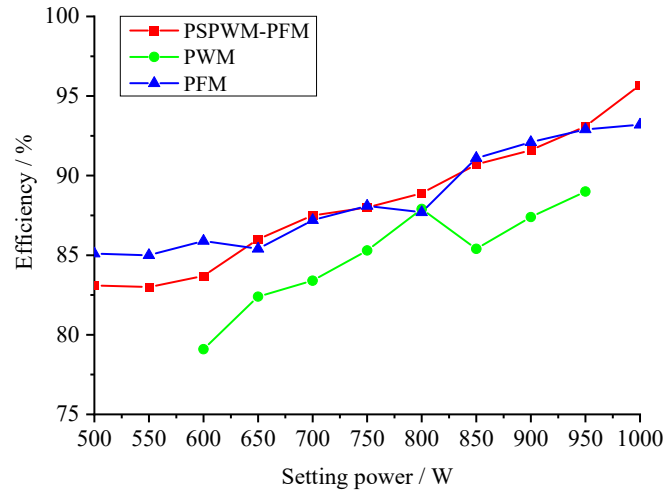

Figure 22. Efficiency curve.

Similarly, according to the recorded experimental data, power matching curves of three modulation modes can be calculated under each set power. Power matching refers to the ratio between the actual output power and the users set power. The closer the value is to 100%, the higher the matching degree is, and the lower the actual output power is. The higher the actual output power is, the higher the actual output power is, as shown in Figure 23. The power matching degree of the PWM modulation mode is the best among the three. This is because the output power is most relevant to the duty cycle. The PFM modulation mode is the worst among the three, especially at low power and high power. This is because the correlation between output power and working frequency is low, and the modulation effect is not obvious. Once the equipment needs a low-power or high-power operation, it will be very difficult.
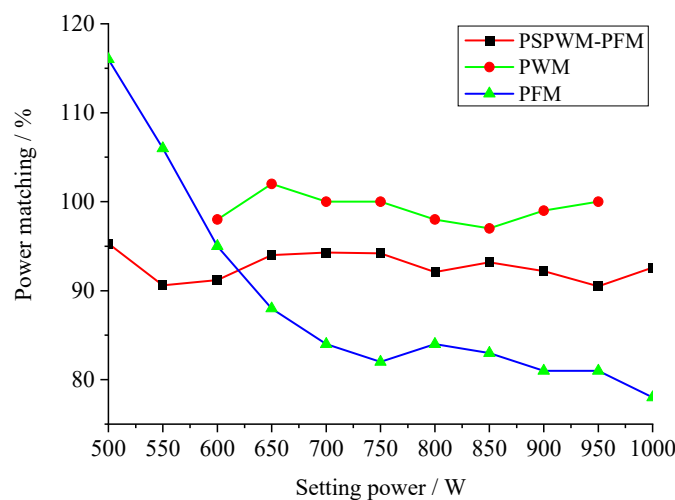

Figure 23. Power matching curve.

Although PFM and PWM modulations are superior to hybrid modulation in a certain aspect such as low power operation, the PFM algorithm is more efficient. The PWM algorithm has a higher power matching accuracy in each power. However, considering efficiency, power matching accuracy, and working power range, the hybrid modulation

algorithm is obviously superior to the other two modulation methods. Therefore, it is appropriate and efficient to select the hybrid modulation algorithm as the control mode of the resonant power supply system for plasma cleaning.

The cover plate of a glass mobile phone was taken as the test object, and the contact angle measuring instrument was used to fix the acting distance at 1.5 cm. The air pressure was 0.15 MPa, the neutral gas temperature was 85 °C, the working frequency was 25 kHz, the processing speed was 100 mm/s, the resonant inductance was 34 mH, and the working gas was compressed air. The contact angle before and after the cover plate was cleaned at different powers and was measured, as shown in Figure 23. The contact angle here refers to the angle formed when the liquid phase is sandwiched between the two tangents of the gas–liquid interface and the solid–liquid interface. As shown in Figure 24, the contact angle decreases gradually with the increase in the set power, indicating that the hydrophilicity of the material is greatly improved, and the cleaning effect of the resonant power supply system for plasma cleaning meets the requirements.

In order to further study the influence of working distance on cleaning effect, the power was set to 500 W~1000 W, and the working distance was set to 0.5 cm~2.5 cm, respectively. The change of contact angle before and after cleaning of the mobile phone cover plate is measured and recorded, as shown in Table 5.

Table 5. Data table of plasma cleaning mobile phone cover plate.

Setting Power (W)	Contact Angle Change Angle (°)				
	0.5 cm	**1 cm**	**1.5 cm**	**2 cm**	**2.5 cm**
500	87.14	78.14	68.92	58.62	39.47
600	92.93	86.74	71.52	63.14	60.59
700	95.83	93.69	77.76	73.28	67.24
800	98.65	96.75	85.13	80.48	73.57
900	103.76	99.94	91.28	85.74	78.18
1000	104.83	101.46	94.08	88.65	82.72

The data in Table 5 are arranged into curves as shown in Figure 25. The analysis shows that the change angle of the contact angle is positively correlated with the set power, that is, the higher the set power, the better the cleaning effect. This negatively correlated with the acting distance, that is, the larger the acting distance, the worse the cleaning effect. However, the contact angle of the mobile phone cover plate after cleaning has a lower limit, that is, there is a minimum contact angle, its value is about 12°, that is, the maximum change angle of the contact angle is about 105°. When the contact angle of the mobile phone cover is close to the maximum value, no matter how the set power increases and how the acting distance decreases, the change of the contact angle will not increase, that is, the contact angle will not decrease after cleaning.

The working distance was set to a fixed value of 1.5 cm, and the power was set to 500 W~1000 W, respectively. Under the same test conditions, two materials, glass and aluminum, were tested. The change data of the material contact angle before and after cleaning are shown in Table 6.

The data in Table 6 are arranged into the curve shown in Figure 26, and the analysis shows that the properties of the acting materials have a significant impact on the cleaning effect. In the same case, under the action of plasma, glass material is obviously more easily activated than aluminum material, the surface free energy is more easily improved, and the flatness changes more, that is, it is easier to be modified.
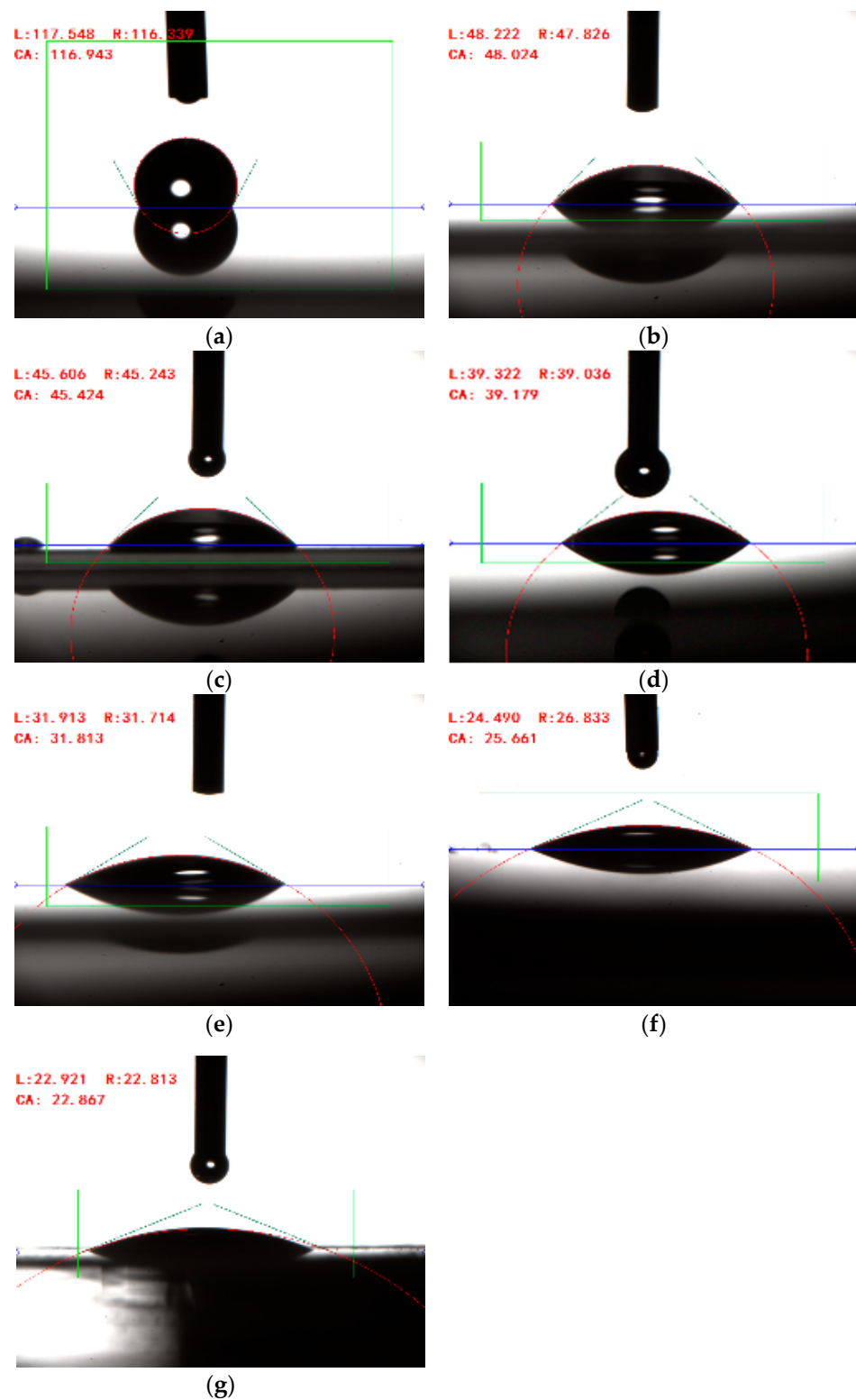
Figure 24. Contact angle of the mobile phone cover; (**a**) Contact angle before cleaning; (**b**) 500 W Contact angle after cleaning; (**c**) 600 W Contact angle after cleaning; (**d**) 700 W Contact angle after cleaning; (**e**) 800 W Contact angle after cleaning; (**f**) 900 W Contact angle after cleaning; and (**g**) 1000 W Contact angle after cleaning.
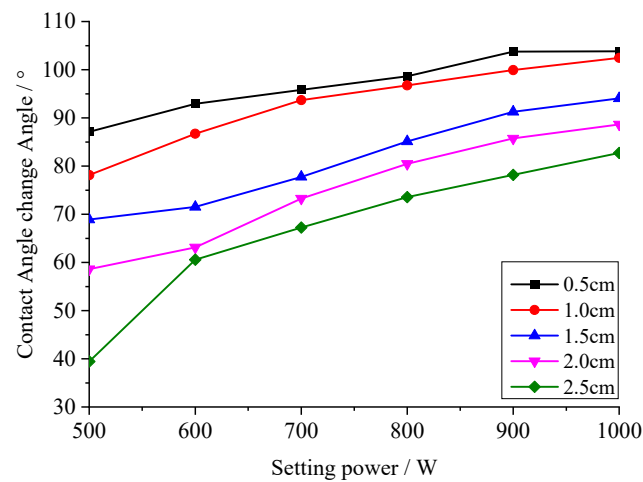
Figure 25. Contact angle curve of the mobile phone cover.

Table 6. Data sheet of glass and aluminum materials for plasma cleaning.

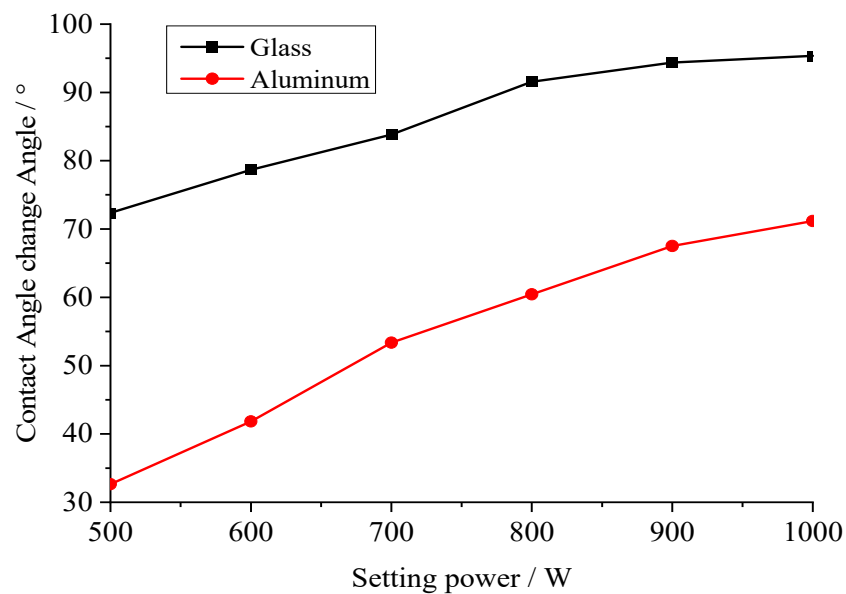| Setting Power (W)	Contact Angle Change Angle (°)	
	Glass	Aluminum
500	72.38	32.66
600	78.68	41.84
700	83.83	53.37
800	91.55	60.44
900	94.37	67.51
1000	95.35	71.17

Figure 26. Contact angle curves of glass and aluminum.

5. Conclusions

In this section, based on the previous sections, a resonant power prototype for plasma cleaning is developed, and an experimental platform is set up to carry out relevant verification experiments:

(1) By comparing and analyzing the advantages and disadvantages of traditional control methods, the control strategy of the PSPWM-PFM hybrid modulation is developed according to the closed-loop program control diagram of the system. The control

method not only has the advantages of PSPWM quick tuning and a wide tuning range, but also has the advantages of PFM to adjust the frequency, prevent the system from deviating from the resonant frequency point, and maintain a high efficiency.

(2) In order to prevent the system from deviating from the resonant frequency and keep the active power output near the maximum value under the current duty ratio, a maximum power tracking algorithm based on fuzzy PFM was developed, and the membership function and fuzzy rules in the fuzzy controller were designed. A simulation model is built to verify the hybrid modulation algorithm and the maximum power tracking algorithm based on fuzzy PFM. Simulation results show that the hybrid modulation algorithm has a fast response speed and a high control precision. The fuzzy PFM maximum power tracking algorithm has a strong anti-perturbation performance and a good tracking performance.

(3) The power adjustment experiment of the hybrid modulation algorithm is carried out to verify the relationship between the output active power, phase shift angle, and the frequency mentioned above. The hybrid modulation, PWM modulation, and PFM modulation algorithms are compared from three aspects of efficiency, power tuning range, and power matching accuracy. It is proved that the hybrid modulation algorithm is feasible and efficient. Its output efficiency is 83.0~95.7%, the power tuning range is 500 W~1000 W, and the output power accuracy is 90~94%.

(4) A plasma cleaning prototype is developed and tested on the experimental platform. The test results meet the design requirements. Among them, the key circuit waveform and control signal precision test results are consistent with the expected. The efficiency of the whole machine ranges from 83% to 95.7%. It performs better at high power above 850 W, and the efficiency is above 90%. The power range is 500 W~1000 W, which solves the problem of arc starting difficulty at low power and overload protection easily triggered at high power. The output power matching accuracy is 90~94%, has an excellent performance, and is suitable for a variety of applications.

Author Contributions: X.C.: methodology, formal analysis, writing—original draft; Z.F.: supervision; H.X.: writing—review and editing, supervision; J.X.: project administration, funding acquisition; D.D. and N.O.: investigation; G.Z.: data curation. All authors have read and agreed to the published version of the manuscript.

Institutional Review Board Statement: Not applicable.

Data Availability Statement: All data, models, and code generated or used during the study appear in the submitted article.

Conflicts of Interest: Authors declare no conflict of interest.

References

1. Luo, H.; Wang, Z. A new ultrasonic cleaning model for predicting the flux recovery of the UF membrane fouled with humic acid. *J. Environ. Chem. Eng.* **2022**, *10*, 107156. [CrossRef]
2. Stephan, U.; Steinke, O.; Ushakov, A.; Verlaan, A.; Yatsuka, E.; Yokoyama, M.; Rijfers, A.; Ribeiro, D.; Moser, L.; Bassan, M.; et al. Design and analysis of first mirror plasma cleaning electrical circuit for Edge Thomson scattering ITER diagnostics. *Fusion Eng. Des.* **2022**, *177*, 113079. [CrossRef]
3. Wu, L.; Liu, Z.; Zhang, W.; Feng, X. Plasma cleaning under low pressures based on the domestic microwave oven. *J. Microw. Power Electromagn. Energy* **2021**, *55*, 128–139. [CrossRef]
4. Li, Y.; Bai, Q.; Yang, D.; Zhang, P.; Lu, L.; Zhang, F.; Yuan, X. Mechanism and Verification of Plasma Cleaning of Organic Contaminant on Aluminum Alloy Surface. *China Surf. Eng.* **2020**, *33*, 58–67. [CrossRef]

5. Li, Y.; Hsieh, M.; Liou, R. Tracking controller design of a RF matching box with plasma load varying. In Proceedings of the 2019 International Aegean Conference on Electrical Machines and Power Electronics (ACEMP) & 2019 International Conference on Optimization of Electrical and Electronic Equipment (OPTIM), Istambul, Turkey, 27 August 2019; pp. 610–615.

6. Wu, S.; Liu, X. Research on Airborne Power Conversion Based on Phase-Shifting Full-Bridge. In *Proceedings of the 11th International Conference on Computer Engineering and Networks*; Liu, Q., Liu, X., Chen, B., Zhang, Y., Peng, J., Eds.; Springer: Singapore, 2022; pp. 942–950.

7. Erni, I.R.; Vidal-Idiarte, E.; Calvente, J.; Guasch-Pesquer, L. Small Signal Modelling for Variable Frequency Control With Maximum Efficiency Point Tracking of DAB Converter. *IEEE Access* **2021**, *9*, 85289–85299. [CrossRef]

8. Wang, Z.; Wang, Y.; Yan, J.; Zhang, K.; Lin, F.; Xiang, L.; Deng, L.; Guan, Z.; Cui, W.; Zhang, H. Pharmaceutical electrospinning and 3D printing scaffold design for bone regeneration. *Adv. Drug Delivery Rev.* **2021**, *174*, 504–534. [CrossRef] [PubMed]

9. Zhang, J.; Zhang, X.; Xia, G.; Zhang, Y.; Di, L. Cold plasma for preparation of Pd/C catalysts toward formic acid dehydrogenation: Insight into plasma working gas. *J. Catal.* **2021**, *400*, 338–346. [CrossRef]

10. Gao, J.; Zhang, J.; Song, Q.; Zhu, Z.; Qian, L. An LLC Resonant Single-Stage Inverter with High-Frequency Link and Soft-Switching. *IEEE J. Emerg. Sel. Top. Power Electron.* **2021**. [CrossRef]

11. Nagai, S.; Nagura, H.; Nakaoka, M.; Okuno, A. High-frequency inverter with phase-shifted PWM and load-adaptive PFM control strategy for industrial induction-heating. In Proceedings of the 28th Annual Meeting of the IEEE Industry Applications Conference, Toronto, ON, Canada, 3–8 October 1993; 1993; Volume 3, pp. 2165–2172.

12. Wang, L.; Yu, X.; Lei, M.; Yin, X. Novel phase-locked loop-based resonant frequency tracking control for linear reciprocating compressor. *Int. J. Low-Carbon Technol.* **2021**, *16*, 1254–1263. [CrossRef]

13. Kivimaki, J.; Kolesnik, S.; Sitbon, M.; Suntio, T.; Kuperman, A. Revisited Perturbation Frequency Design Guideline for Direct Fixed-Step Maximum Power Point Tracking Algorithms. *IEEE Trans. Ind. Electron.* **2017**, *64*, 4601–4609. [CrossRef]

14. Veerapen, S.; Wen, H.; Li, X.; Du, Y.; Yang, Y.; Wang, Y.; Xiao, W. A novel global maximum power point tracking algorithm for photovoltaic system with variable perturbation frequency and zero oscillation. *Sol. Energy* **2019**, *181*, 345–356. [CrossRef]

15. Hemalatha, N.; Seyezhai, R. Implementation of fuzzy MPPT controller for PV-based three-phase modified capacitor-assisted extended boost q-ZSI. *Appl. Nanosci.* **2022**. [CrossRef]

16. Tian, H.; Peng, S.; Jia, Y.; Zhang, T.; Yan, C. Research on precise driving control of rover based on adaptive fuzzy controller. In *6th International Conference on Automation, Control and Robotics Engineering, CACRE 2021, 15–17 July 2021*; Institute of Electrical and Electronics Engineers Inc.: Dalian, China, 2021; pp. 285–289.

17. Chaturvedi, D.K.; Umrao, R.; Malik, O.P. Adaptive polar fuzzy logic based load frequency controller. *Int. J. Electr. Power Energy Syst.* **2015**, *66*, 154–159. [CrossRef]

18. Bozhko, V.I.; Naumenko, E.V.; Kornyushko, V.F.; Biglov, R.R. Synthesis of Fuzzy Algorithms Controlling the Temperature of the Polymer in the Extruder. In *Intelligent Algorithms in Software Engineering*; Silhavy, R., Ed.; Springer International Publishing: Cham, Switzerland, 2020; pp. 484–491.

19. Meesrisuk, W.; Jangwanitlert, A.; Suwan-Ngam, W. A PSPWM with variable frequency control for a two-output three-level series resonant inverter. In *12th International Conference on Electrical Engineering/Electronics, Computer, Telecommunications and Information Technology, ECTI-CON 2015, 24–27 June 2015*; Institute of Electrical and Electronics Engineers Inc.: Changwat Prachuap Khiri Khan, Thailand, 2015.

20. Liu, L.; Yang, Y.; Zhu, Z. A High Efficiency PWM/PFM Dual-mode DC/DC Switching Regulator. *Res. Prog. Solid State Electron.* **2006**, *26*, 209–213. [CrossRef]